



A *Ziziphus jujuba* waste-derived biochar as a low-cost adsorbent for the removal of Indigo carmine dye from aqueous solution

Sara Satouh^{a,b}, Salim Bousba^{c,d,*}, Nabil Bougdah^{b,e}, Charf Eddine Bounoukta^{f,g}, Sabrina Halladja^a, Nabil Messikh^b

^aDépartement de Chimie, Faculté des Sciences, Université 20 Août 1955-Skikda, Algérie, emails: s.satouh@univ-skikda.dz (S. Satouh), s.halladja@univ-skikda.dz (S. Halladja)

^bLaboratoire de Recherche Sur La Physico-chimie Des Surfaces Et Interfaces, Faculté Des Sciences, Université 20 Août 1955, Skikda, Algérie, emails: n.bougdah@univ-skikda.dz (N. Bougdah), nabchem@yahoo.fr (N. Messikh)

^cDépartement de Génie des Procédés, Faculté de Génie des Procédés, Université Salah Bounider Constantine 3, Algérie

^dLaboratoire Médicament et Développement Durable (ReMeDD), Université Constantine 3, Constantine, Algérie, email: salim.bousba@univ-constantine3.dz (S. Bousba)

^eDépartement de Génie des procédés, Faculté de Technologie, Université 20 Août 1955-Skikda, Algérie

^fDepartamento de Química Inorgánica e Instituto de Ciencia de Materiales de Sevilla – Centro Mixto CSIC/Universidad de Sevilla, Avda. Américo Vespucio, 49, 41092, Sevilla, Spain

^gLaboratoire de Génie des Procédés Chimiques-LGPC, Département de Génie des Procédés, Faculté de Technologie, Université FERHAT ABBAS SETIF-1, 19000, Setif, Algeria, email: charfeddinebounoukta@gmail.com (C.E. Bounoukta)

Received 2 November 2022; Accepted 5 March 2023

ABSTRACT

In this work, a local Algerian agricultural waste biomass, *Ziziphus jujuba*, was valorized into a new low-cost biochar (JB). The biochar was produced by a simple pyrolysis at 700°C for 1 h under an inert atmosphere and was used as a low-cost adsorbent to remove Indigo carmine dye (IC) from aqueous solution. The JB biochar was characterized by Fourier-transform infrared spectroscopy, scanning electron microscopy-energy-dispersive X-ray spectroscopy, X-ray diffraction, Raman, pH_{pzc} and Brunauer–Emmett–Teller physico-chemical techniques. Adsorption studies were conducted using a batch process to study the effects of contact time, adsorbent amount, initial IC dye concentration, initial pH, ionic strength, and temperature. The Langmuir, Freundlich, and Temkin isotherm models were used to analyze equilibrium adsorption data, while the pseudo-first-order, pseudo-second-order, Elovich, and intraparticle diffusion models were used to analyze kinetic data. The equilibrium data was well fitted to the Freundlich isotherm with an R^2 value of 0.974. The theoretical maximum adsorption capacity was found to be 166.46 mg/g at 20°C according to the Langmuir model. The adsorption kinetic was found to follow the pseudo-first-order kinetic model. Thermodynamic study showed that the adsorption of IC onto JB biochar was feasible, spontaneous and endothermic.

Keywords: *Ziziphus jujuba*; Biochar; Adsorbent; Indigo carmine; Isotherms; Kinetic; Thermodynamic

* Corresponding author.

1. Introduction

The widespread use of organic dyes in various industries, such as food, textiles, and cosmetics, has led to the release of large amounts of industrial wastewater into the environment without proper treatment [1–3]. These wastewater effluents contain highly toxic and non-degradable azo and aromatic structures which can harm the ecological environment and human health [4,5].

Indigo carmine (IC) is a synthetic dye found naturally in the so-called *Indigofera tinctoria* plant that was discovered as early as 1600 B.C. [6]. The IC anionic dye can be used in multi-industries such as textile, food, pharmaceutical, cosmetics, and paper for the coloration of their product [7–11] as well as it has been used in the field of biology as microscope stains and indicator for analytical chemistry domain research [12]. However, the industrial effluent in water is highly toxic and leads to serious environmental issues, and can harm ecosystems even at low concentrations [13]. The contact of IC with the human body can affect the skin and eyes by irritation and cause permanent injury to the cornea as well as conjunctive [14]. IC can also provoke gastrointestinal irritation that leads to vomiting, nausea, and diarrhea [15]. Therefore, the immediate treatment of IC harmful pollutants in the wastewater after deposit is essential.

Several processes have been proposed for the elimination of IC dye from wastewater, such as electrolysis [16,17], ultrafiltration [18,19], photochemical [20,21], electrocoagulation [22,23], biological [24–26], and adsorption methods [27–29]. Among mentioned, the adsorption method appears as one of the best alternatives for removing complex aromatic molecular indigo matter due to its simplicity of low-cost operating and available maintenance design [28–30].

The effectiveness of the adsorption process largely depends on the nature of adsorbent especially pore size distribution, porosity, and surface area [31]. The selection of the appropriate solid material is crucial for the successful implementation of adsorption-based purification techniques. Various natural and synthetic adsorbents have been used to eliminate dyes from synthetic wastewater. These materials include clays/zeolites and their composites [32], biosorbents [33], agricultural solid wastes [34], industrial by-products and their composites [35], metal organic frameworks [36], and miscellaneous materials [37]. Recently, biochar which is a carbonaceous material derived from biomass has gained increasing attention due to its desirable properties, such as a high content of porous structures and a large specific area, good cation exchange capacity, hydrophobicity, and non-corrosiveness. As a result, biochar has emerged as an excellent adsorbent for removing pollutants from wastewater [38,39]. Additionally, biochar can play a vital role in improving environmental management and developing sustainable energy production [40].

Most carbonaceous matters from biomass are obtained by pyrolysis thermochemical process in an oxygen-limited environment [41]. Many organic wastes, different temperature ranges, and controlled flow of various gases are used as pyrolysis parameter conditions for the development of new adsorbents-based biochar.

Thus, carbon materials from *Ziziphus jujuba* (ZJ) are especially attractive adsorbents. The ZJ is abundant, readily

available at a low cost, and presents excellent thermochemical resistance, which can yield a large quantity of final matter with the required structural textural properties [42].

The aim of this study is the synthesis of adsorbent material derived from agricultural waste biomass, namely, *Ziziphus jujuba* (ZJ) by a simple pyrolysis method, which has the advantages of low cost and ease of operation. To the best of our knowledge, this is the first study to explore the use of the ZJ based biochar for indigo carmine removal from water. The present work lies in the exploration of a new, sustainable and cost-effective adsorbent material for the removal of indigo carmine dye from water.

The structure-textural properties analyses are investigated by Fourier-transform infrared spectroscopy (FTIR), scanning electron microscopy-energy-dispersive X-ray spectroscopy (SEM-EDX), X-ray diffraction (XRD), Raman, and Brunauer–Emmett–Teller (BET) physicochemical techniques. At the same time, the effect of the adsorption media parameters like contact time, adsorbent amount, initial dye concentration, initial pH, ionic strength, and temperature have been performed with the goal of achievement of high IC adsorption capacity. For further, various kinetic and isotherm models and thermodynamic studies are carried out to state the adsorption mechanism of the IC dye on the biochar.

2. Materials and methods

2.1. Chemicals

Indigo carmine commonly known as Acid Blue 74 is a water-soluble powder with a purple color, having a molecular formula of $C_{16}H_8O_8N_2S_2Na_2$ (with a molecular weight of 466.36 mg/g), which was obtained from (Merck KGaA, Germany) and used as procured. A 1,000 mg/L stock solution of the dye was prepared using deionized water.

2.2. Adsorbent preparation

In this study, *Ziziphus jujuba* (ZJ), one of the most abundant agricultural wastes in the Mediterranean region, was used as a raw material to derive a carbon-based adsorbent. ZJ was collected from the Skikda region in the northeast of Algeria, washed with distilled water, and air-dried for several days. The dried sample was ground and sieved to obtain a reduced particle size (0.5–1 mm) and was subsequently used to prepare the biochar sample.

The biochar preparation from raw ZJ was carried out by heat treatment pyrolysis process in a tubular steel furnace, with operating conditions of 5°C/min heating rate, 100 cm³/min nitrogen flow rate, and maximum temperature of 700°C for 1 h. After pyrolysis, the obtained biochar is neutralized and washed using 0.1 M HCl, then laved several times with distilled water and finally dried at 100°C for 24 h. The final obtained biochar is labeled (JB).

2.3. Characterization

Scanning electron microscopy (SEM) images are performed in a HITACHI S-4800 microscope (Hitachi, Ltd., Japan) FEG-fitted with secondary and back-scattered

electron detectors. The compositional analysis was obtained with microanalysis energy-dispersive X-ray spectroscopy (EDX), operating at a working distance of 15 mm, and a voltage of 2 kV. The micrographs were taken at a 4 mm working distance and 20 kV voltage.

XRD patterns are made at room temperature on a PANalytical X'Pert Pro diffractometer (Malvern PANalytical Ltd., UK) with copper K α radiation at a wavelength of 1.541 Å, operated at 45 kV and 40 mA. Diffractograms were performed with a 2 θ range from 10° to 90°, with a step size of 0.05° and a time per step of 300 s. The crystalline phases' structural parameters determination: inter-layer spacing (d_{002}), The aromatic layer stacking heights (L_c), lateral size (L_a), and the average number of aromatic layers per carbon crystallite (N_{avg}) (defined graphically according to Li et al. [43] were calculated by the followed equations using Bragg' and Scherrer empirical equations [44].

$$d_{002} = \frac{\lambda}{2 \sin \theta_{002}} \quad (1)$$

$$L_c = \frac{K_c \lambda}{\beta_{002} \cos \theta_{002}} \quad (2)$$

$$L_a = \frac{K_a \lambda}{\beta_{100} \cos \theta_{100}} \quad (3)$$

$$N_{avg} = \frac{L_c}{d_{002}} + 1 \quad (4)$$

where λ is the wavelength of the X-radiation (1.541 Å); θ_{002} or θ_{100} is the Bragg diffraction angle of the (002) or (100) plane; β_{002} or β_{100} is the full width of the (002) or (100) peaks at half maximum intensity (FWHM), and K_c or K_a is a shape factor depending on the diffracted plane (0.89 for the (002) and 1.84 for (100)).

FTIR spectrum of the JB biochar was performed in a Shimadzu FTIR 8400 (Shimadzu, Japan) having a standard mid-IR DTGS detector using the KBr pellets technique. The spectra was recorded between 4,000 and 400 cm^{-1} .

Raman measurements are performed on a HR800 Horiba Jobin Yvon dispersive microscope (HORIBA, Ltd., Japan) with a confocal aperture of 1,000 μ , a laser spot diameter of 0.72 μ , and a spatial resolution of 360 nm. The microscope is equipped with 600 tours/mm diffraction grating using a CCD detector, a green laser ($\lambda = 532.14$ nm) working at 20 mW maximum power, and a 100 \times objective.

The textural properties measurement of the JB biochar adsorbent is carried out by the liquid nitrogen adsorption-desorption tests measurements at 77 K temperature in Micromeritics ASAP 2010 equipment (Micromeritics, Inc., USA). Previously, the sample is degassed at 350°C for 12 h in a vacuum.

The determination of the pH at the point of zero charge (pH_{pzc}) was conducted using drift method [45] by adjusting the pH of 50 mL/0.01 mol/L NaCl solutions to values between 2 and 10. JB biochar of 0.025 g were added and the final pH was measured after 24 h under agitation. The

pH_{pzc} is the point where $\text{pH}_f - \text{pH}_i = 0$ (i.e., the intersection along the initial pH axis).

2.4. Adsorption studies

Batch adsorption experiments were performed to study the effects of contact time (5–400 min), adsorbent amount (10–100 mg), initial dye concentration (1–20 mg/L), temperature (20°C–60°C), and initial pH (2–12) on the removal of IC dye. The batch experiments were carried out in Erlenmeyer flasks, adding 0.045 g of adsorbent and 500 mL of IC solutions. Then the flasks are placed on a rotary shaker at 300 rpm and the samples are taken at regular time intervals and centrifuged at (5,000 rpm). The IC content in the supernatant liquid is determined and analyzed on a UV-visible spectrophotometer (Analytik Jena, Germany) with the maximum wavelength of 610 nm. The amount of IC adsorbed on JB biochar q_e (mg/g) is calculated according to the following equation:

$$q_e = \frac{(C_0 - C_e)V}{m} \quad (5)$$

where C_0 and C_e are the initial and equilibrium or residual IC concentrations, respectively (mg/L). V is the volume of IC solution (L), and m is the mass of adsorbent (g). The IC removal percentage $R(\%)$ was calculated by the following formula:

$$R(\%) = \frac{(C_0 - C_e)}{C_0} \times 100 \quad (6)$$

3. Results and discussion

3.1. Characterization of the JB biochar

3.1.1. Morphology analysis by SEM-EDX

Firstly, the pyrolysis effect on the surface structure of the prepared carbon biochar is carried out by SEM-EDX. The luminous region in the images corresponds to the minerals of ash impurities in the final obtained carbon material. The JB sample, pictures in Fig. 1. show that there are fragments found on the surface structure of JB with separated aggregates and high nearby low pores size developments.

Herein, elements content analysis by EDX of the JB (Table 1) reveals that in the company of high carbon content (87.17 wt.%), with limited oxygen (6.98 wt.%). Different minerals and chlorine arises from the natural source. The inorganic matter release with more oxygen load can improve the polarity and hydrophilicity of biochar properties [46] and allows for a more accessible porous surface.

3.1.2. XRD, Raman and FTIR analysis

The different crystalline phase's diffractograms of JB adsorbent analyzed by XRD are shown in Fig. 2.

In typical of the amorphous carbon materials, two distinct characteristic peaks of the 002 plane 20°–25° and 100 plane 40°–45° 2 θ . The mentioned plane is dedicated respectively to the amorphous and the graphitic carbon. Besides,

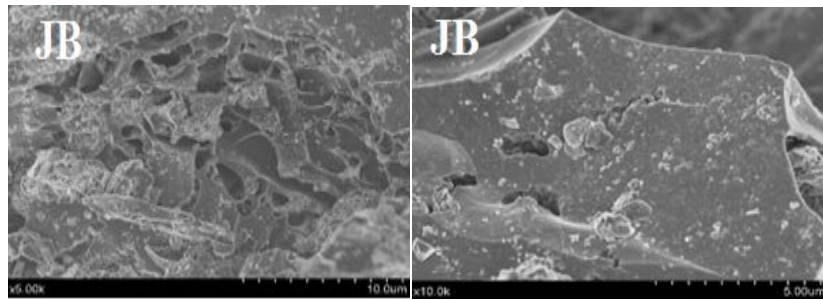


Fig. 1. Scanning electron microscopy images of JB biochar.

Table 1

Element composition of the prepared JB biochar analyzed by scanning electron microscopy-energy-dispersive X-ray spectroscopy

Element	wt. %
C	87.17
O	6.98
Al	0.09
Si	0.06
P	0.29
Cl	2.23
K	0.13
Ca	1.76
Fe	1.3

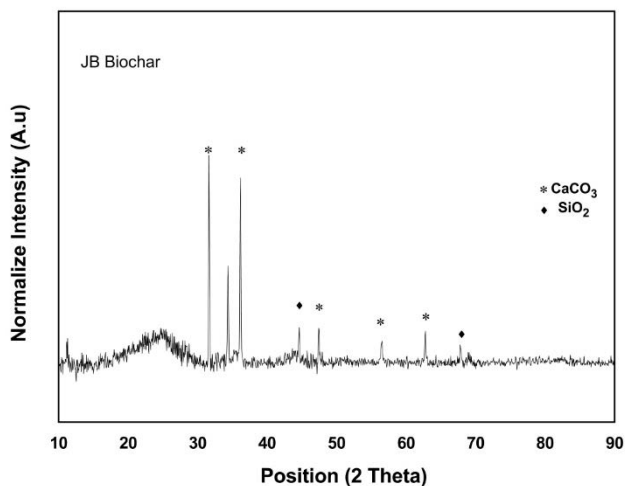


Fig. 2. X-ray diffraction patterns of the JB biochar.

the peaks at around $80^\circ 2\theta$ of the (110) plane correspond also to the turbostratic state structure of the carbon. The sharps peaks are contributed to the different minerals crystalline phases presented in the carbon biochar as well as calcium carbonate CaCO_3 (Rhombohedral, ICDD 00-005-0586) and silicon oxide SiO_2 (Hexagonal, ICDD 00-046-1045) from X'Pert HighScore patterns by comparison with PDF2 ICDD2000 (Powder Diffraction File 2 International Center for Diffraction Data, 2000) database.

Table 2

Structural parameters calculated from X-ray diffraction and Raman

Sample	JB biochar
L_c (nm)	1.25
L_a (nm)	105.84
N	4.4
d_{002} (nm)	0.36
Crystallite size (nm)	1.32
I_D/I_G	0.87

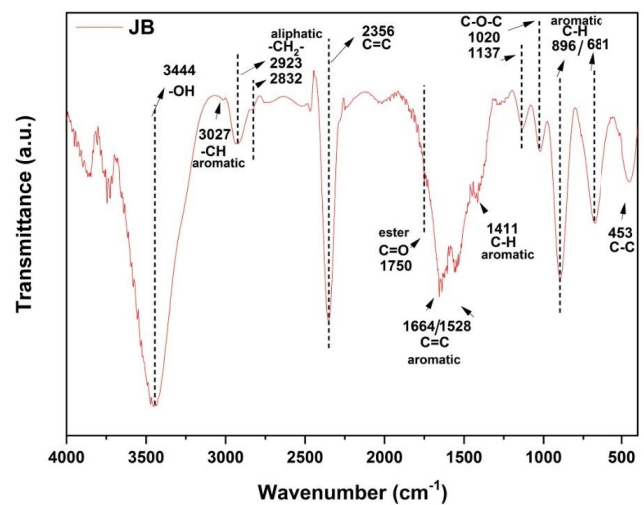


Fig. 3. Fourier-transform infrared spectra for JB biochar.

The carbon crystallite parameters were calculated and are listed in Table 2. The average means number of crystallite carbon of the JB biochar is calculated to be in the range of 4–5. The inter-planar spacing d_{002} is highly superior to 0.36 (graphite crystallite), corroborating that the sample is far from graphitization and is disordered [47].

The length of the separated graphitic aggregates crystallite is low, in contrast to the lateral size of the crystallite L_a which is very high.

The analyzed functional groups by FTIR spectra are shown in Fig. 3. The broad absorption band at absorbance superior to $3,100 \text{ cm}^{-1}$ with a maximum at about $3,344 \text{ cm}^{-1}$

is characteristic of the O–H stretching of the adsorbed water and phenol carboxyl groups [48]. The bands at around $3,027\text{ cm}^{-1}$ were assigned to $-\text{CH}$ stretching in aromatic structures [49]. Bands centered at $2,923/2,832\text{ cm}^{-1}$ were attributed to asymmetric/symmetric C–H bending in the aliphatic structure, respectively. The bands at $2,356\text{ cm}^{-1}$ could be attributed to (C=C) vibration in alkyne groups [50]. The band at $1,750\text{ cm}^{-1}$ was related to C=O stretching of carboxylic groups [51]. Bands at $1,664$ and $1,528\text{ cm}^{-1}$ are related to C=C stretching in aromatic structures of the carbon lignin Z] part; the absorption band at $1,411\text{ cm}^{-1}$ was assigned to an aromatic ring-like C–C stretching mode in polyaromatics [52]. Bands at $1,137$ and $1,020\text{ cm}^{-1}$ are related to C–O–C stretching in aromatic rings, and the bands at 453 cm^{-1} are associated with C–C stretching [53]. The bands at 896 and 681 cm^{-1} mean the vibration of aromatic C–H out-of-plane bending [54].

Raman spectroscopy is used for the determination of the structural defects in the carbon-based materials; the spectra display two distinct peaks Fig. 4. D-band ($1,340\text{ cm}^{-1}$) and G-band ($1,600\text{ cm}^{-1}$), are generally assigned respectively to zone center phonons of E_{2g} symmetry and K-point phonons of A_{1g} symmetry [55]. The peaks are expected to the graphite structure defects and graphitic layers in the biochar, respectively [56]. The intense G band manifests and corroborates with FTIR analysis the presence of high sp^2 hybridization, while the D band appearance in the Raman shift is linked to the sp^3 hybridizations existence and defects degree [57]. The I_D/I_G ratio can be used to describe the disorder degree of biochar. The I_D/I_G intensity ratio for the JB biochar is equal to 0.87, indicating the disordered structure of carbons.

3.1.3. Specific surface area and pore structural characterization analysis

The texture properties analysis by N_2 adsorption–desorption isotherms of JB biochar is shown in Fig. 5. Adsorption–desorption curves belong to typical type I of the

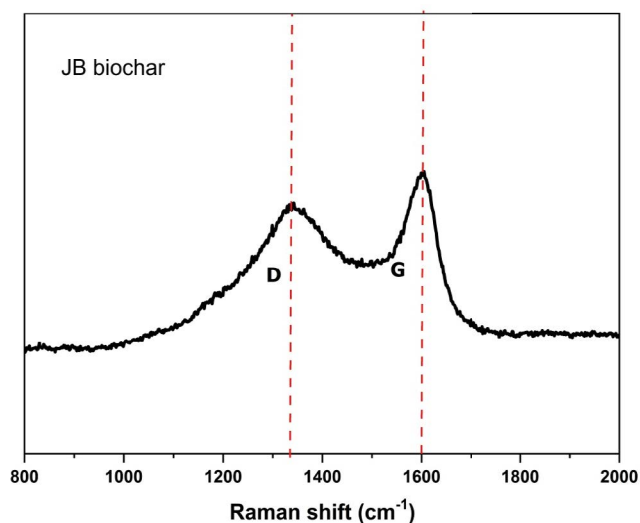


Fig. 4. Raman spectra for JB biochar.

Langmuir model, indicating the presence of microporous structures [58].

The specific surface area is calculated using the BET equation, while sizes and pore distribution were determined by Barrett–Joyner–Halenda (BJH) method using the desorption curve.

Herein, all the calculated texture parameters summarized in Table 3 show high values data for our JB biochar. The BET surface area was $368.6\text{ m}^2/\text{g}$. In fact, a mesoporous surface is developed with a limited accessible microporous surface. Likewise, the calculated means average pores diameter by BJH method of mesopores is equal to 3.0 nm . Interestingly, high specific surface area and more mesoporous structure depicted more active site exposure and were beneficial for high adsorption capacities [59].

3.1.4. Determination of the pH of the point of zero charge

The pH of the point of zero charge (pH_{pzc}) refers to the pH value at which the surface of a material has a neutral charge and there is an equal number of positively and negatively charged species present. The pH_{pzc} of a material is dependent on its chemical composition and the functional groups on its surface. The result for the determination of pH_{pzc} of JB biochar is shown in Fig. 6. From Fig. 6, the pH_{pzc} value is approximately 8.26. Therefore, the surface of JB biochar was a negatively charged at pH over this value and positively charged at pH below this value. The obtained pH_{pzc} value

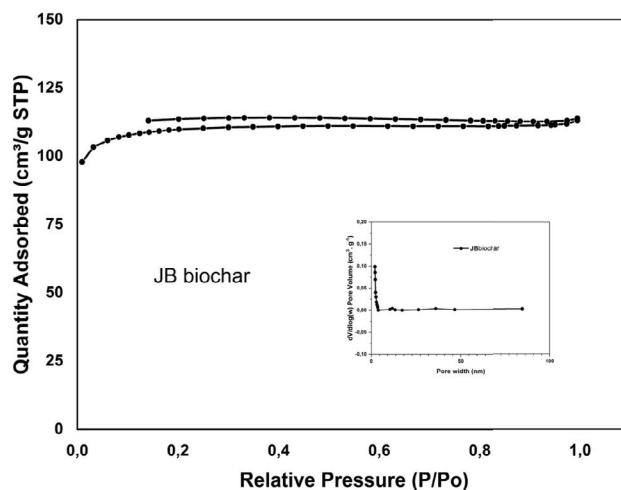


Fig. 5. N_2 adsorption–desorption isotherms for JB biochar.

Table 3
Calculated textural parameters of JB biochar

Biochar	JB
Brunauer–Emmett–Teller surface area (m^2/g)	368.6
Barrett–Joyner–Halenda pore volume (cm^3/g)	0.013
Pore diameter (nm)	3.0
Mesoporous surface (m^2/g)	325
Microporous surface (m^2/g)	0.123

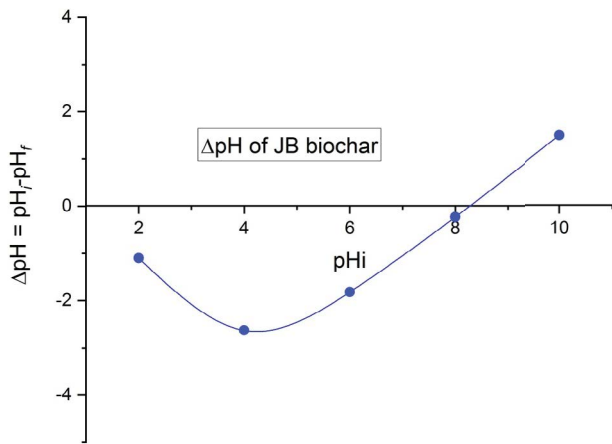


Fig. 6. Determination of pH_{pzc} using drift method.

of the JB biochar is in agreement with the values obtained for biochars in the literature [60,61].

3.2. Adsorption studies results

3.2.1. Effect of contact time on adsorption equilibrium

Fig. 7. show the result of dynamic adsorption of IC dye onto JB biochar. In the beginning, the adsorption increased rapidly until equilibrium was reached at about 300 min. The initial rapid rate of IC adsorption probably due to the availability of a large number of active sites for adsorption and the following decrease may be due to the saturation of the adsorption sites and attainment of equilibrium [42]. In the process application, the quicker adsorption phenomenon is useful since the shorter contact time effectively achieves for a smaller size of the contact equipment, which in turn directly affects both the operation cost and capacity of the process [62].

3.2.2. Effect of the amount of adsorbent

The effect of the mass of biochar on the adsorption of IC was studied by varying the mass of the adsorbent from (10–100 mg). It was seen (Fig. 8.) that the removal of IC increases on increasing the mass of the biochar due to an increase in the number of active sites [63]. Beyond 45 mg of adsorbent, the IC removal remains unchanged and the adsorption capacity of the adsorbent starts to decrease. Therefore, a mass of 45 mg was selected as the optimal adsorbent dose and used for all sets of experiments.

3.2.3. Effect of temperature

The influence of temperature on the adsorption of IC dye from water is analyzed by varying the temperature between 293 and 333 K. It was clear (Fig. 9.) that increasing temperature led to an increase in the amount of IC dye adsorbed at equilibrium. Such an increase in the adsorption capacity of IC dye may either be due to the creation of some new active sites on the adsorbent surface or to the acceleration of some originally slow adsorption steps [42].

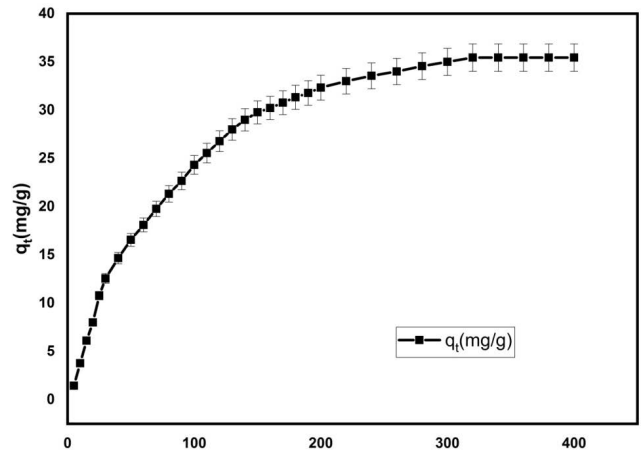


Fig. 7. Effect of contact time on the adsorption of Indigo carmine dye onto JB biochar.

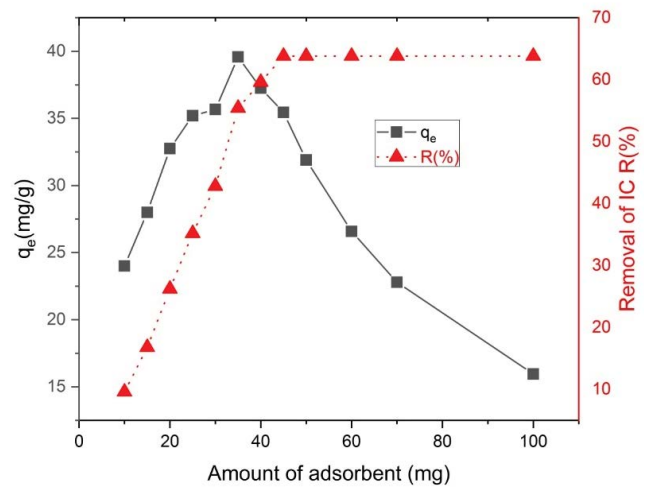


Fig. 8. Effect of the adsorbent amount on the adsorption of Indigo carmine dye.

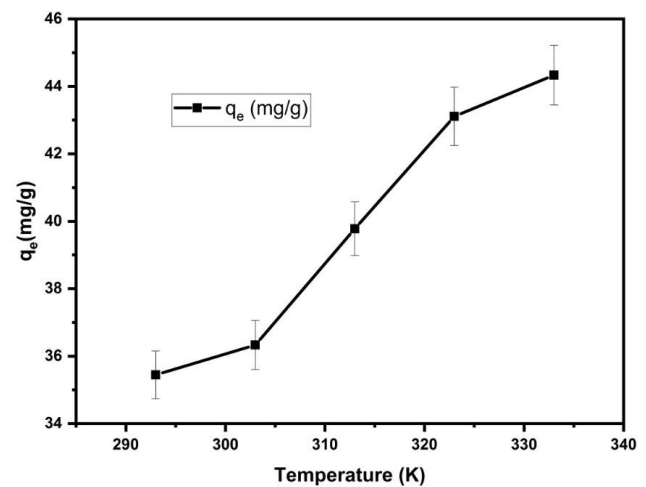


Fig. 9. Effect of temperature on the adsorption of Indigo carmine by JB biochar.

3.2.4. Effect of IC dye initial concentration

Fig. 10 illustrates the impact of various initial IC concentrations on both the adsorption yield and equilibrium uptake capacity. The experimental findings indicate that adsorption efficiency decreases with an increase in initial dye concentration, while the equilibrium uptake capacity increases. At lower concentrations, all dye ions in the solution interact with the binding sites of the adsorbent. However, each adsorbent has a finite number of binding sites that become saturated at a particular concentration [64]. At higher concentrations, the binding sites reach their saturation point, leading to a decrease in removal efficiency and more unabsorbed IC ions in the solution. In contrast, the uptake capacity increases with the initial dye concentration as the driving force required for the mass transfer resistance of the dye ions to be retained on the adsorbent surface is enhanced by the concentration gradient [65].

3.2.5. Effect of initial pH

The pH is an important parameter in wastewater treatment by adsorption processes because it can influence both the ionization of surface functional groups of the adsorbent and the chemical structure of the solution. The adsorption of IC dye by JB biochar at different pH values showed that the adsorption capacities are slightly affected by pH in the range from 2 to 8 and then decrease sharply (Fig. 11). For $pH \leq pH_{pzc}$ and since the dye is negatively charged ($pH < pKa$) possibly the acidic solution favors adsorption of the dye onto the biochar surface, which acquires positive charge in acidic solution as predicted by the pH_{pzc} [66,67]. In fact, at $pH < pH_{pzc}$ attractive columbic forces occurred between the biochar surface and anionic IC molecules, hence the high adsorption capacity [68,69]. On the other hand, at $pH > pH_{pzc}$ the hydroxyl (OH^-) ions in the aqueous solution compete effectively with the dye anions, causing a decrease in the adsorption capacity [70].

3.2.6. Effect of ionic strength

The presence of electrolytes in a solution may influence the strength of adsorbate–adsorbent interactions [47],

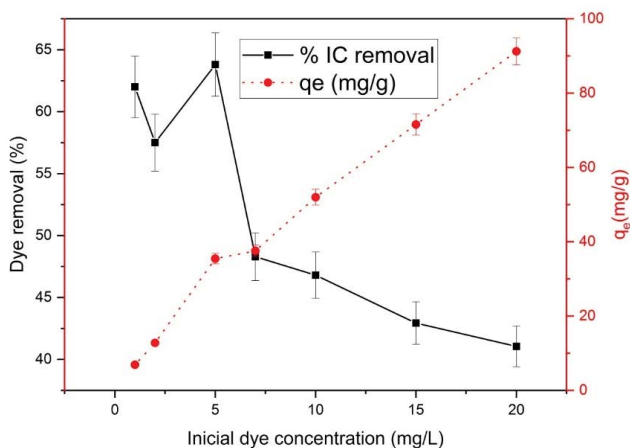


Fig. 10. Effect of Indigo carmine dye initial concentration.

hence the effect of NaCl monovalent salt concentration on IC dye adsorption was studied. As shown in Fig. 12, when the NaCl concentration increased from 0 to 500 mg/L, the adsorption amount of IC dye onto JB biochar decreased slightly from 35.44 to 27.95 mg/g. This suggests that electrolytes may compete with IC molecules for adsorption on JB during the adsorption process, which confirms the existence of electrostatic interactions between IC molecules and the JB surface. However, the relatively small reduction in the adsorption capacity (21%) of IC dye with the increase in salt concentration suggests that electrostatic interactions are not the only mechanism responsible for the adsorption of IC dye on JB.

3.3. Adsorption kinetics

The kinetic analysis of the adsorption process is mainly explained by four kinetic models: pseudo-first-order,

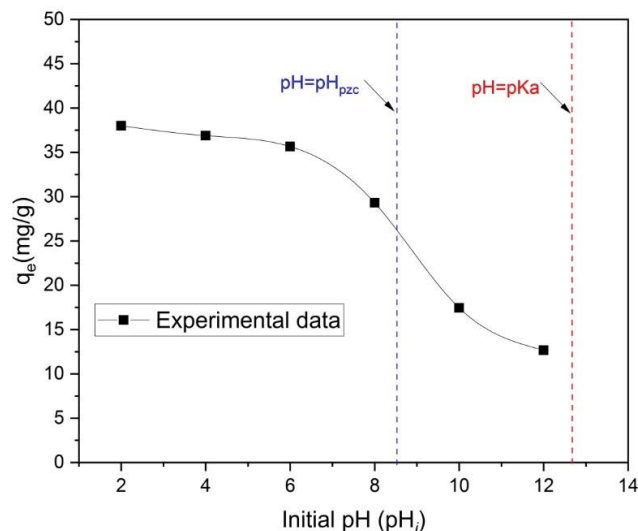


Fig. 11. Effect of initial pH.

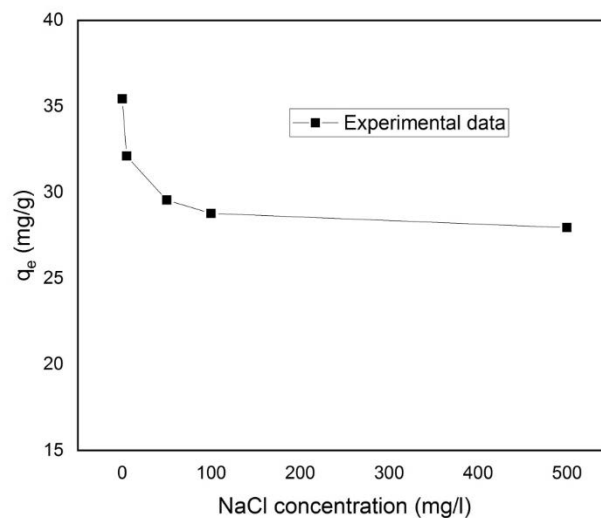


Fig. 12. Effect of ionic strength.

pseudo-second-order, Elovich, and intraparticle diffusion models [Eqs. (7)–(9), respectively] [71].

$$q_t = q_e (1 - e^{-k_1 t}) \tag{7}$$

$$q_t = \frac{k_2 q_e^2 t}{1 + k_2 q_e t} \tag{8}$$

$$q_t = \frac{1}{\beta} \ln(\alpha \beta t + 1) \tag{9}$$

$$q_t = K_{id} \times \sqrt{t} + C \tag{10}$$

where q_e and q_t are the amounts of adsorbed IC at equilibrium and at time t , respectively; k_1 , k_2 , and k_{id} are the equilibrium rate constants for pseudo-first-order, pseudo-second-order, and intraparticle diffusion models, respectively. C is a constant, and α and β are the Elovich coefficients.

The goodness of the models is determined by the correlation coefficient (R^2) and the standard error for each parameter. The parameters of each model as well as R^2 are shown in Table 4, and the resulting curves are shown in Fig. 13.

Data obtained from kinetic studies is fitted to the pseudo-first-order model better than the others models due to the high R^2 value. Further, the calculated value of equilibrium adsorption capacity (35.709 ± 0.227 mg/g) using the pseudo-first-order equation is similar to the experimentally determined value (i.e., 35.44 mg/g).

Since the pseudo-first-order model did not suggest a definite mechanism for adsorption, the results were analyzed using the intraparticle diffusion model. As seen from the plot pattern of q_t vs. $t^{1/2}$ (Fig. 14), there are three stages in terms of the intraparticle diffusion kinetic model. The plot is not passing through the origin, implying that the intraparticle diffusion is not the only rate control step, and the boundary layer diffusion may also influence the adsorption process. The first stage is characterized by fast adsorption process owing to the surface adsorption by boundary layer diffusion; while the second stage which is characterized by

slow adsorption process represented intra particulate diffusion. In the third stage the equilibrium adsorption was reached. This result revealed that the adsorption process was controlled by two steps; rapid surface adsorption and slow intra particle diffusion stage [72,73].

The parameters of intraparticle diffusion model are calculated by linear regression for the three stages and presented in Table 5.

The intraparticle diffusion rate constant for the first stage k_{d1} is higher than the same constant for the second stage k_{d2} and at the same time C_2 is higher than C_1 illustrated that the removal rate of dye in the first stage was higher than that in the second stage.

3.4. Adsorption isotherms

The equilibrium adsorption characteristics of IC onto biochar was explained by the adjustment of the experimental isotherms to Langmuir, Freundlich and Temkin models [74].

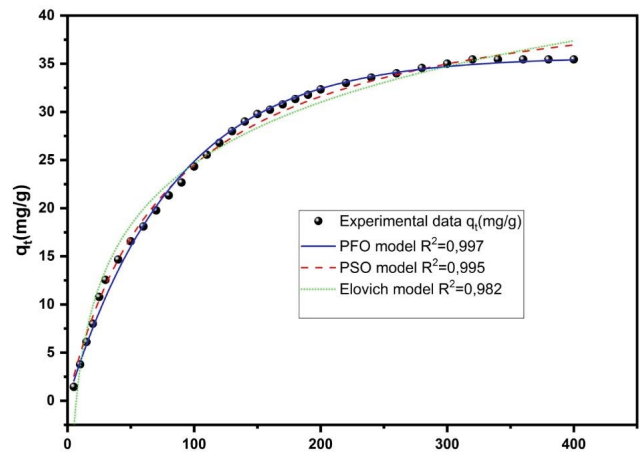


Fig. 13. Kinetic models of Indigo carmine adsorption on JB biochar.

Table 4
Kinetic parameters of Indigo carmine adsorption onto JB biochar

Model	Parameter and unit	Value
Pseudo-first-order	$q_{e,exp}$ (mg/g)	35.44
	$q_{e,cal}$ (mg/g)	35.709 ± 0.227
	k_1 (min^{-1})	$0.012 \pm 2.319\text{E-}4$
	R^2	0.997
Pseudo-second-order	$q_{e,cal}$ (mg/g)	44.475 ± 0.532
	k_2 (g/mg·min)	$2.759\text{E-}4 \pm 1.313\text{E-}5$
	R^2	0.995
Elovich	α	0.492 ± 0.024
	β	0.109 ± 0.002
	R^2	0.982

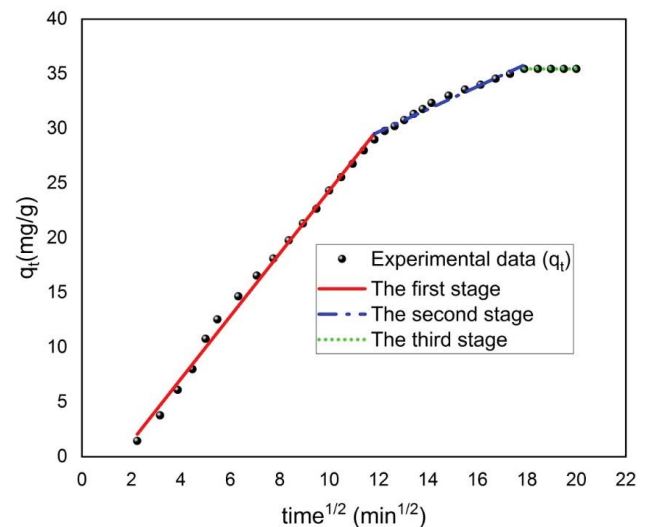


Fig. 14. Intraparticle diffusion model for Indigo carmine dye adsorption.

Eq. (11) describes the Langmuir’s isotherm.

$$q_e = \frac{q_{\max} K_L C_e}{1 + K_L C_e} \tag{11}$$

where q_{\max} (mg/g) represents the maximum amount within a monolayer and C_e (mg/L) is the equilibrium concentration. K_L (L/mg) is the Langmuir’s isotherm constant which is related to the adsorption energy. The dimensionless separation factor was calculated using Eq. (12).

$$R_L = \frac{1}{1 + C_i K_L} \tag{12}$$

where R_L is a dimensionless parameter, which indicates the adsorption possibility either favorable ($0 < R_L < 1$), unfavorable ($R_L > 1$), linear adsorption ($R_L = 1$) or irreversible ($R_L = 0$). The nonlinear plot of q_e vs. C_e for Langmuir model is shown in Fig. 15.

Eq. (13) represents the Freundlich model:

$$q_e = K_F \times C_e^{1/n} \tag{13}$$

where K_F is the Freundlich constant, is related to the affinity of the adsorbent to the adsorbate, and $1/n$ (dimensionless) gives an indication on the favorable nature of the adsorption. In reality, the Freundlich exponent ($1/n$) explains the type of isotherm, when ($1/n > 1$) the adsorption is unfavorable, ($1/n = 1$) the adsorption is homogeneous and ($0 < 1/n < 1$) the adsorption is favorable [75]. The nonlinear plot of the adsorption capacity at equilibrium q_e vs. the C_e for Freundlich’s isotherm is shown in Fig. 15.

The Temkin’s isotherm describes the behavior of adsorption process on heterogeneous surfaces. The nonlinear plot of q_e vs. C_e for Temkin model is shown in Fig. 15.

Eq. (14) represents the Temkin model:

$$q_e = B \ln(AC_e) \tag{14}$$

Table 5
Intraparticle diffusion model parameters for Indigo carmine adsorption

Intraparticle diffusion stages	Parameter and unit	Value
First stage	k_{d1} (mg/(g·t ^{1/2}))	2.867 ± 0.051
	C_1 (mg/g)	-4.364 ± 0.409
	$(R_1)^2$	0.995
Second stage	k_{d2} (mg/(g·t ^{1/2}))	1.038 ± 0.042
	C_2 (mg/g)	17.241 ± 0.625
	$(R_2)^2$	0.982
Third stage	k_{d3} (mg/(g·t ^{1/2}))	–
	C_3 (mg/g)	35.444 ± 1E-14
	$(R_3)^2$	–

where A (L/g) is the Temkin’s isotherm equilibrium binding constant, and B (J/mol) is the constant related to heat of sorption.

The values of R^2 and the parameters obtained from Langmuir, Freundlich and Temkin models are shown in Table 6. The results indicated that the Freundlich model gives a better fit on the basis of the correlation coefficient values (R^2).

When Langmuir, Freundlich, and Temkin models are evaluated together, the experimental results were more compatible to the Freundlich isotherm model due to the highest R^2 value that it exhibits. As it is seen from Table 6, the IC adsorption process onto JB biochar is favorable because of the fact that $1/n$ value was smaller than 1.

3.5. Adsorption thermodynamics

Thermodynamic constants are calculated using the following equations:

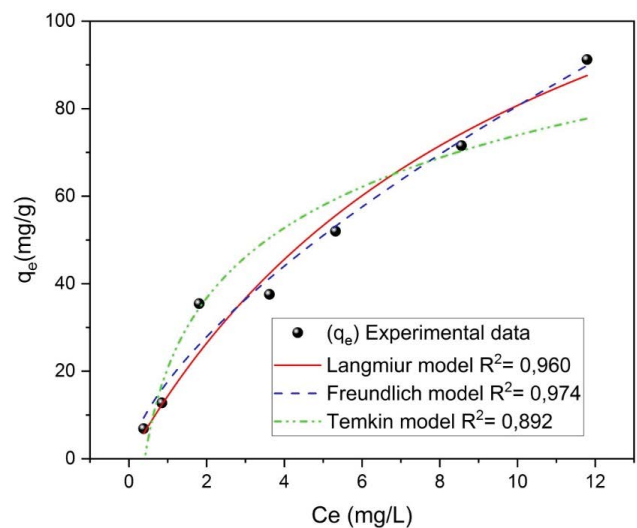


Fig. 15. Langmuir, Freundlich and Temkin models of Indigo carmine adsorption on JB biochar.

Table 6
Langmuir, Freundlich and Temkin parameters for Indigo carmine adsorption onto JB biochar

Model	Parameter and unit	Value
Langmuir	q_{\max} (mg/g)	166.456 ± 38.655
	K_L	0.094 ± 0.037
	R^2	0.960
	R_L	[0.912–0.342]
Freundlich	K_F	17.627 ± 2.310
	$1/n$	0.660 ± 0.062
	R^2	0.974
Temkin	B (J/mol)	23.134 ± 3.236
	A (L/mg)	2.443 ± 0.764
	R^2	0.910

Table 7
Thermodynamic parameters estimation at three temperatures

Adsorbent	Temp. (K)	K_d	ΔG° (kJ/mol)	ΔH° (kJ/mol)	ΔS° (J/mol)	R^2
JB	293	19.58	-7.246	16.31 ± 1.66	80.20 ± 5.33	0.989
	313	28.01	-8.672			
	333	43.89	-10.47			

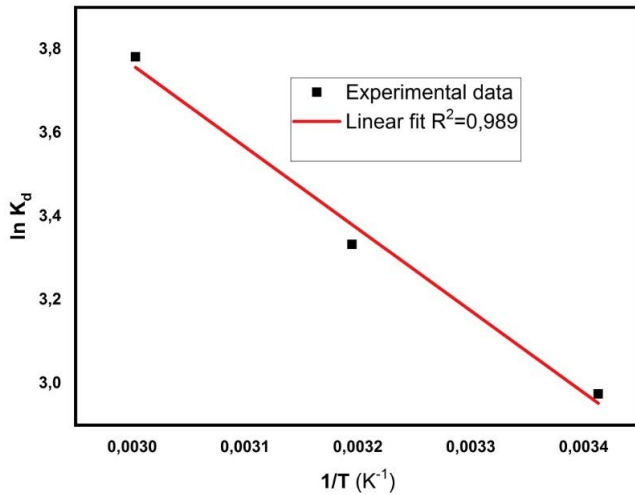


Fig. 16. Plot of $\ln K_d$ vs. $1/T$ for the adsorption of Indigo carmine onto JB biochar.

$$K_d = \frac{q_e}{C_e} \quad (15)$$

$$\Delta G^\circ = -RT \ln K_d \quad (16)$$

$$\ln K_d = \frac{\Delta S^\circ}{R} - \frac{\Delta H^\circ}{RT} \quad (17)$$

where ΔG° , ΔH° and ΔS° are standard free energy change, standard entropy change and standard enthalpy change respectively, K_d is the equilibrium constant, T is the adsorption temperature on Kelvin scale and R is the ideal gas constant (8.314 J/mol·K). ΔH° and ΔS° were determined from slope and intercept of a van't Hoff plot of $\ln K_d$ vs. the reciprocal of temperature as shown in Fig. 16. The estimated thermodynamic parameters of IC removal by biochar are shown in Table 7. It can be observed that the values of ΔG° decreased with the rise in temperature from 293 to 333 K. The negative values of ΔG° confirm the spontaneity and feasibility of the process. It can also be seen that the values of ΔG° become more negative with the increase in temperature which revealed that the adsorption process was more favorable at higher temperatures. The positive ΔH° and ΔS° values suggested that the adsorption reaction was endothermic. The positive value of ΔS° (80.20 kJ/mol) indicates the increased randomness at the solid-solution interface during the adsorption process [76].

Table 8
Comparison of adsorption capacity of various adsorbents in the removal of Indigo carmine dye

Adsorbent	q_{\max} (mg/g)	References
JB biochar	166.46	This work
MgFe ₂ O ₄ nanoparticles	46.08	[77]
<i>Chromolaena odorata</i> biochar	98.8	[29]
Mg/Fe LDH nanoparticles	55.5	[78]
Peanut shell activated carbon (AC)	82.64	[79]
Crab shell chitosan (CH)	96.15	[79]
Prepared chitosan/activated carbon (CH/AC)	208.33	[79]
Commercial activated carbon (CAC)	79.49	[28]

3.6. Comparison with reported adsorbents

To evaluate the effectiveness of the JB biochar to remove IC dye from water, a comparison of the adsorption capacity with other relevant studies is presented in Table 8. Based on the results, it can be concluded that the value of q_{\max} obtained in this work is in good agreement with most previous studies, indicating that IC can be efficiently adsorbed on the JB biochar.

Furthermore, the high adsorption capacity observed in this study can be attributed to the presence of mesopores. These mesopores provide suitable binding sites for IC with high affinity, thus enhancing the overall adsorption performance of the JB [29,77,78]. The presence of mesopores also allows for easy access of the IC molecules to the active sites within the JB, resulting in a rapid adsorption process [80].

4. Conclusion

In this work, JB biochar was prepared from ZJ waste using a simple and cost-effective pyrolysis method without any chemical activation. The obtained JB biochar was used as an efficient adsorbent for IC dye removal from water. The physicochemical features of the biochar were investigated using SEM-EDX, XRD, FTIR, Raman, and BET studies. BET analysis revealed a high specific surface area with a mesoporous structure which is beneficial for high adsorption capacities of IC molecules. Batch adsorption experiments showed the successful removal of IC dye on JB biochar at a wide pH range. The prepared biochar shows quite good adsorption efficiency for IC dye removal, with an equilibrium adsorption capacity of 166.46 mg/g at 20°C. These

experimental equilibrium data were investigated and fitted well with the Freundlich isotherm. Furthermore, the kinetic data obeyed pseudo-first-order kinetics. The estimated thermodynamic parameters indicated that the IC removal process was endothermic and was accompanied by increasing the random arrangement of IC molecules on a biochar surface. The negative ΔG° values reflected a spontaneous adsorption that become more favorable at higher temperatures. The obtained results confirmed that the prepared JB biochar compared well with the previously reported adsorbents. Additionally, the high adsorption capacity of the JB biochar, in combination with its low-cost production and environmental sustainability, highlights its potential as a promising adsorbent for the removal of IC from wastewater.

References

- [1] S. Yadav, K.S. Tiwari, C. Gupta, M.K. Tiwari, A. Khan, S.P. Sonkar, A brief review on natural dyes, pigments: recent advances and future perspectives, *Res. Chem.*, 5 (2023) 100733, doi: 10.1016/j.rechem.2022.100733.
- [2] A.A. Khan, J. Gul, S.R. Naqvi, I. Ali, W. Farooq, R. Liaqat, H. Al-Mohamadi, L. Štěpánek, D. Juchelková, Recent progress in microalgae-derived biochar for the treatment of textile industry wastewater, *Chemosphere*, 306 (2022) 135565, doi: 10.1016/j.chemosphere.2022.135565.
- [3] V. Kumar, P. Saharan, A.K. Sharma, A. Umar, I. Kaushal, A. Mittal, Y. Al-Hadeethi, B. Rashad, Silver doped manganese oxide-carbon nanotube nanocomposite for enhanced dye-sequestration: isotherm studies and RSM modelling approach, *Ceram. Int.*, 46 (2020) 10309–10319.
- [4] R. Kishor, D. Purchase, G.D. Saratale, R.G. Saratale, L.F.R. Ferreira, M. Bilal, R. Chandra, R.N. Bharagava, Ecotoxicological and health concerns of persistent coloring pollutants of textile industry wastewater and treatment approaches for environmental safety, *J. Environ. Chem. Eng.*, 9 (2021) 105012, doi: 10.1016/j.jece.2020.105012.
- [5] P. Saharan, V. Kumar, J. Mittal, V. Sharma, A.K. Sharma, Efficient ultrasonic assisted adsorption of organic pollutants employing bimetallic-carbon nanocomposites, *Sep. Sci. Technol.*, 56 (2021) 2895–2908.
- [6] M.F. Chowdhury, S. Khandaker, F. Sarker, A. Islam, M.T. Rahman, Md.R. Awwal, Current treatment technologies and mechanisms for removal of indigo carmine dyes from wastewater: a review, *J. Mol. Liq.*, 318 (2020) 114061, doi: 10.1016/j.molliq.2020.114061.
- [7] J. Wang, L. Lu, F. Feng, Improving the indigo carmine decolorization ability of a *Bacillus amyloliquefaciens* laccase by site-directed mutagenesis, *Catalysts*, 7 (2017) 275, doi: 10.3390/catal7090275.
- [8] J. Mittal, Permissible synthetic food dyes in India, *Resonance*, 25 (2020) 567–577.
- [9] L. Kavieva, G. Ziyatdinova, Voltammetric sensor based on SeO_2 nanoparticles and surfactants for indigo carmine determination, *Sensors*, 22 (2022) 3224, doi: 10.3390/s22093224.
- [10] S.A. Patil, P.D. Kumbhar, S.K. Patil, M.M. Vadiyar, U.P. Suryawanshi, C.L. Jambhale, M.A. Anuse, J.H. Kim, S.S. Kolekar, Dynamic adsorption of toxic indigo carmine dye on bio-inspired synthesised Fe_3O_4 nanoparticles: kinetic and thermodynamic study, *Int. J. Environ. Anal. Chem.*, 102 (2022) 1205–1227.
- [11] D. Sikdar, S. Goswami, P. Das, Activated carbonaceous materials from tea waste and its removal capacity of indigo carmine present in solution: synthesis, batch and optimization study, *Sustainable Environ. Res.*, 30 (2020) 30, doi: 10.1186/s42834-020-00070-8.
- [12] A.H. Gemeay, I.A. Mansour, R.G. El-Sharkawy, A.B. Zaki, Kinetics and mechanism of the heterogeneous catalyzed oxidative degradation of indigo carmine, *J. Mol. Catal. A: Chem.*, 193 (2003) 109–120.
- [13] R. Zein, L. Hevira, Zilfa, Rahmayeni, S. Fauzia, J.O. Ighalo, The improvement of indigo carmine dye adsorption by *Terminalia catappa* shell modified with broiler egg white, *Biomass Convers. Biorefin.*, (2022), doi: 10.1007/s13399-021-02290-3.
- [14] A. Mittal, J. Mittal, L. Kurup, Batch and bulk removal of hazardous dye, indigo carmine from wastewater through adsorption, *J. Hazard. Mater.*, 137 (2006) 591–602.
- [15] A. Kesraoui, T. Selmi, M. Seffen, F. Brouers, Influence of alternating current on the adsorption of indigo carmine, *Environ. Sci. Pollut. Res.*, 24 (2017) 9940–9950.
- [16] S. Hammami, M.A. Oturan, N. Oturan, N. Bellakhal, M. Dachraoui, Comparative mineralization of textile dye indigo by photo-Fenton process and anodic oxidation using boron-doped diamond anode, *Desal. Water Treat.*, 45 (2012) 297–304.
- [17] W. Zhan, Y. Du, J. Lan, R. Lei, R. Li, D. Du, T.C. Zhang, Electrochemical degradation of indigo carmine by low voltage pulse electrolysis, *J. Mol. Liq.*, 348 (2022) 118006, doi: 10.1016/j.molliq.2021.118006.
- [18] D. Cailean, G. Barjoveanu, C.-P. Musteret, N. Sulitanu, L.R. Manea, C. Teodosiu, Reactive dyes removal from wastewater by combined advanced treatment, *Environ. Eng. Manage. J.*, 8 (2009) 503–511.
- [19] M. Hu, S. Yang, X. Liu, R. Tao, Z. Cui, C. Matindi, W. Shi, R. Chu, X. Ma, K. Fang, M. Titus, B.B. Mamba, J. Li, Selective separation of dye and salt by PES/SPSf tight ultrafiltration membrane: roles of size sieving and charge effect, *Sep. Purif. Technol.*, 266 (2021) 118587, doi: 10.1016/j.seppur.2021.118587.
- [20] K.R. Reddy, A.K. Agnihotri, Y. Yukselen-Aksoy, B.K. Dubey, A. Bansal, Eds., *Sustainable Environmental Geotechnics: Proceedings of EGRWSE 2019*, Springer International Publishing, Cham, 2020. Available at: <https://doi.org/10.1007/978-3-030-51350-4>
- [21] M.M. Sousa, C. Miguel, I. Rodrigues, A.J. Parola, F. Pina, J.S. Seixas de Melo, M.J. Melo, A photochemical study on the blue dye indigo: from solution to ancient Andean textiles, *Photochem. Photobiol. Sci.*, 7 (2008) 1353, doi: 10.1039/b809578g.
- [22] D. Donneys-Victoria, D. Bermúdez-Rubio, B. Torralba-Ramírez, N. Marriaga-Cabrales, F. Machuca-Martínez, Removal of indigo carmine dye by electrocoagulation using magnesium anodes with polarity change, *Environ. Sci. Pollut. Res.*, 26 (2019) 7164–7176.
- [23] M.S. Secula, I. Crețescu, S. Petrescu, An experimental study of indigo carmine removal from aqueous solution by electrocoagulation, *Desalination*, 277 (2011) 227–235.
- [24] S. Park, J.-Y. Ryu, J. Seo, H.-G. Hur, Isolation and characterization of alkaliphilic and thermotolerant bacteria that reduce insoluble indigo to soluble leuco-indigo from indigo dye vat, *J. Korean Soc. Appl. Biol. Chem.*, 55 (2012) 83–88.
- [25] A. Paz, J. Carballo, M.J. Pérez, J.M. Domínguez, Biological treatment of model dyes and textile wastewaters, *Chemosphere*, 181 (2017) 168–177.
- [26] M. Ramya, B. Anusha, S. Kalavathy, Decolorization and biodegradation of Indigo carmine by a textile soil isolate *Paenibacillus larvae*, *Biodegradation*, 19 (2008) 283–291.
- [27] R.M. Ferreira, N.M. de Oliveira, L.L.S. Lima, A.L.D.M. Campista, D.M.A. Stapelfeldt, Adsorption of indigo carmine on *Pistia stratiotes* dry biomass chemically modified, *Environ. Sci. Pollut. Res.*, 26 (2019) 28614–28621.
- [28] Z. Harrache, M. Abbas, T. Aksil, M. Trari, Thermodynamic and kinetics studies on adsorption of indigo carmine from aqueous solution by activated carbon, *Microchem. J.*, 144 (2019) 180–189.
- [29] E.C. Nnadozie, P.A. Ajibade, Isotherm, kinetics, thermodynamics studies and effects of carbonization temperature on adsorption of indigo carmine (IC) dye using *C. odorata* biochar, *Chem. Data Collect.*, 33 (2021) 100673, doi: 10.1016/j.cdc.2021.100673.
- [30] M.B. Ahmad, U. Soomro, M. Muqet, Z. Ahmed, Adsorption of indigo carmine dye onto the surface-modified adsorbent prepared from municipal waste and simulation using deep neural network, *J. Hazard. Mater.*, 408 (2021) 124433, doi: 10.1016/j.jhazmat.2020.124433.

- [31] A. Mariyam, J. Mittal, F. Sakina, R.T. Baker, A.K. Sharma, A. Mittal, Efficient batch and fixed-bed sequestration of a basic dye using a novel variant of ordered mesoporous carbon as adsorbent, *Arabian J. Chem.*, 14 (2021) 103186, doi: 10.1016/j.arabjc.2021.103186.
- [32] Ü. Ecer, A. Zengin, T. Şahan, Magnetic clay/zeolitic imidazole framework nanocomposite (ZIF-8@Fe₃O₄@BNT) for reactive orange 16 removal from liquid media, *Colloids Surf., A*, 630 (2021) 127558, doi: 10.1016/j.colsurfa.2021.127558.
- [33] Aruna, N. Bagotia, A.K. Sharma, S. Kumar, A review on modified sugarcane bagasse biosorbent for removal of dyes, *Chemosphere*, 268 (2021) 129309, doi: 10.1016/j.chemosphere.2020.129309.
- [34] S. Afroz, T.K. Sen, A review on heavy metal ions and dye adsorption from water by agricultural solid waste adsorbents, *Water Air Soil Pollut.*, 229 (2018) 225, doi: 10.1007/s11270-018-3869-z.
- [35] F. Marrakchi, B.H. Hameed, M. Bouaziz, Mesoporous and high-surface-area activated carbon from defatted olive cake by-products of olive mills for the adsorption kinetics and isotherm of methylene blue and acid blue 29, *J. Environ. Chem. Eng.*, 8 (2020) 104199, doi: 10.1016/j.jece.2020.104199.
- [36] C. Arora, S. Soni, P.K. Bajpai, J. Mittal, A. Mariyam, Chapter 14 – Dye Removal From Wastewater Using Metal Organic Frameworks, P. Singh, C.M. Hussain, S. Rajkhowa, Eds., *Management of Contaminants of Emerging Concern (CEC) in Environment*, Elsevier, Amsterdam, The Netherlands, 2021, pp. 375–394. Available at: <https://doi.org/10.1016/B978-0-12-822263-8.00014-2>
- [37] H. Daraei, A. Mittal, Investigation of adsorption performance of activated carbon prepared from waste tire for the removal of methylene blue dye from wastewater, *Desal. Water Treat.*, 90 (2017) 294–298.
- [38] J. Wang, S. Wang, Preparation, modification and environmental application of biochar: a review, *J. Cleaner Prod.*, 227 (2019) 1002–1022.
- [39] P. Zhang, H. Sun, L. Min, C. Ren, Biochars change the sorption and degradation of thiocloprid in soil: insights into chemical and biological mechanisms, *Environ. Pollut.*, 236 (2018) 158–167.
- [40] H.S. Kambo, A. Dutta, A comparative review of biochar and hydrochar in terms of production, physico-chemical properties and applications, *Renewable Sustainable Energy Rev.*, 45 (2015) 359–378.
- [41] N. Kaya, Z.Y. Uzun, Investigation of effectiveness of pinecone biochar activated with KOH for methyl orange adsorption and CO₂ capture, *Biomass Convers. Biorefin.*, 11 (2021) 1067–1083.
- [42] H.D. Bouras, O. Benturki, N. Bouras, M. Attou, A. Donnot, A. Merlin, F. Addoun, M.D. Holtz, The use of an agricultural waste material from *Ziziphus jujuba* as a novel adsorbent for humic acid removal from aqueous solutions, *J. Mol. Liq.*, 211 (2015) 1039–1046.
- [43] Q. Li, Q. Tao, C. Yuan, Y. Zheng, G. Zhang, J. Liu, Investigation on the structure evolution of pre and post explosion of coal dust using X-ray diffraction, *Int. J. Heat Mass Transfer*, 120 (2018) 1162–1172.
- [44] H. Takagi, K. Maruyama, N. Yoshizawa, Y. Yamada, Y. Sato, XRD analysis of carbon stacking structure in coal during heat treatment, *Fuel*, 83 (2004) 2427–2433.
- [45] Y. Jiao, D. Han, Y. Lu, Y. Rong, L. Fang, Y. Liu, R. Han, Characterization of pine-sawdust pyrolytic char activated by phosphoric acid through microwave irradiation and adsorption property toward CDNB in batch mode, *Desal. Water Treat.*, 77 (2017) 247–255.
- [46] H.I. Yang, K. Lou, A.U. Rajapaksha, Y.S. Ok, A.O. Anyia, S.X. Chang, Adsorption of ammonium in aqueous solutions by pine sawdust and wheat straw biochars, *Environ. Sci. Pollut. Res.*, 25 (2018) 25638–25647.
- [47] W. Zhang, H. Tao, B. Zhang, J. Ren, G. Lu, Y. Wang, One-pot synthesis of carbonaceous monolith with surface sulfonic groups and its carbonization/activation, *Carbon*, 49 (2011) 1811–1820.
- [48] N.V. Sych, S.I. Trofymenko, O.I. Poddubnaya, M.M. Tsyba, V.I. Sapsay, D.O. Klymchuk, A.M. Puziy, Porous structure and surface chemistry of phosphoric acid activated carbon from corncob, *Appl. Surf. Sci.*, 261 (2012) 75–82.
- [49] K. Jindo, H. Mizumoto, Y. Sawada, M.A. Sanchez-Monedero, T. Sonoki, Physical and chemical characterization of biochars derived from different agricultural residues, *Biogeosciences*, 11 (2014) 6613–6621.
- [50] J. Yang, K. Qiu, Preparation of activated carbons from walnut shells via vacuum chemical activation and their application for methylene blue removal, *Chem. Eng. J.*, 165 (2010) 209–217.
- [51] X. Zhao, W. Ouyang, F. Hao, C. Lin, F. Wang, S. Han, X. Geng, Properties comparison of biochars from corn straw with different pretreatment and sorption behaviour of atrazine, *Bioresour. Technol.*, 147 (2013) 338–344.
- [52] A. Ausavasukhi, C. Kamposoen, O. Kengnok, Adsorption characteristics of Congo red on carbonized leonardite, *J. Cleaner Prod.*, 134 (2016) 506–514.
- [53] H. Yang, R. Yan, H. Chen, D.H. Lee, C. Zheng, Characteristics of hemicellulose, cellulose and lignin pyrolysis, *Fuel*, 86 (2007) 1781–1788.
- [54] A.-N.A. El-Hendawy, Variation in the FTIR spectra of a biomass under impregnation, carbonization and oxidation conditions, *J. Anal. Appl. Pyrolysis*, 75 (2006) 159–166.
- [55] A.C. Ferrari, J. Robertson, Interpretation of Raman spectra of disordered and amorphous carbon, *Phys. Rev. B: Condens. Matter*, 61 (2000) 14095–14107.
- [56] B. Li, Y. Zhang, J. Xu, Y. Mei, S. Fan, H. Xu, Effect of carbonization methods on the properties of tea waste biochars and their application in tetracycline removal from aqueous solutions, *Chemosphere*, 267 (2021) 129283, doi: 10.1016/j.chemosphere.2020.129283.
- [57] C.E. Bounoukta, C. Megías-Sayago, S. Ivanova, A. Penkova, F. Ammari, M.A. Centeno, J.A. Odriozola, Effect of the sulphonating agent on the catalytic behavior of activated carbons in the dehydration reaction of fructose in DMSO, *Appl. Catal., A*, 617 (2021) 118108, doi: 10.1016/j.apcata.2021.118108.
- [58] M. Thommes, K. Kaneko, A.V. Neimark, J.P. Olivier, F. Rodriguez-Reinoso, J. Rouquerol, K.S.W. Sing, Physisorption of gases, with special reference to the evaluation of surface area and pore size distribution (IUPAC Technical Report), *Pure Appl. Chem.*, 87 (2015) 1051–1069.
- [59] Y. Hua, T. Jiang, K. Wang, M. Wu, S. Song, Y. Wang, P. Tsiakaras, Efficient Pt-free electrocatalyst for oxygen reduction reaction: highly ordered mesoporous N and S co-doped carbon with saccharin as single-source molecular precursor, *Appl. Catal., B*, 194 (2016) 202–208.
- [60] A. Albalasmeh, M.A. Gharaibeh, O. Mohawesh, M. Alajlouni, M. Quzaih, M. Masad, A. El Hanandeh, Characterization and artificial neural networks modelling of methylene blue adsorption of biochar derived from agricultural residues: effect of biomass type, pyrolysis temperature, particle size, *J. Saudi Chem. Soc.*, 24 (2020) 811–823.
- [61] H. Nguyen Tran, S.-J. You, H.-P. Chao, Effect of pyrolysis temperatures and times on the adsorption of cadmium onto orange peel derived biochar, 34 (2016), doi: 10.1177/0734242X15615698.
- [62] P.X. Sheng, Y.-P. Ting, J.P. Chen, L. Hong, Sorption of lead, copper, cadmium, zinc, and nickel by marine algal biomass: characterization of biosorptive capacity and investigation of mechanisms, *J. Colloid Interface Sci.*, 275 (2004) 131–141.
- [63] S. Bhowmik, V. Chakraborty, P. Das, Batch adsorption of indigo carmine on activated carbon prepared from sawdust: a comparative study and optimization of operating conditions using response surface methodology, *Results Surf. Interfaces*, 3 (2021) 100011, doi: 10.1016/j.rsurfi.2021.100011.
- [64] S. Chowdhury, P. Saha, Seashell powder as a new adsorbent to remove Basic Green 4 (Malachite Green) from aqueous solutions: equilibrium, kinetic and thermodynamic studies, *Chem. Eng. J.*, 164 (2010) 168–177.
- [65] M. Doğan, M. Alkan, Ö. Demirbaş, Y. Özdemir, C. Özmetin, Adsorption kinetics of maxilon blue GRL onto sepiolite from aqueous solutions, *Chem. Eng. J.*, 124 (2006) 89–101.
- [66] S. Sánchez-Rodríguez, J. Trujillo-Reyes, E. Gutiérrez-Segura, M. Solache-Ríos, A. Colin-Cruz, Removal of indigo carmine by

- a Ni nanoscale oxides/*Schoenoplectus acutus* composite in batch and fixed bed column systems, *Sep. Sci. Technol.*, 50 (2015) 1602–1610.
- [67] I. Othman, R.M. Mohamed, I.A. Ibrahim, M.M. Mohamed, Synthesis and modification of ZSM-5 with manganese and lanthanum and their effects on decolorization of indigo carmine dye, *Appl. Catal., A*, 299 (2006) 95–102.
- [68] G.O. Achieng, C.O. Kowenje, J.O. Lalah, S.O. Ojwach, Preparation, characterization of fish scales biochar and their applications in the removal of anionic indigo carmine dye from aqueous solutions, *Water Sci. Technol.*, 80 (2020) 2218–2231.
- [69] A. Badeenezhad, A. Azhdarpoor, S. Bahrami, S. Yousefinejad, Removal of methylene blue dye from aqueous solutions by natural clinoptilolite and clinoptilolite modified by iron oxide nanoparticles, *Mol. Simul.*, 45 (2019) 564–571.
- [70] R. Slimani, I. El Ouahabi, F. Abidi, M. El Haddad, A. Regti, M.R. Laamari, S.E. Antri, S. Lazar, Calcined eggshells as a new biosorbent to remove basic dye from aqueous solutions: thermodynamics, kinetics, isotherms and error analysis, *J. Taiwan Inst. Chem. Eng.*, 45 (2014) 1578–1587.
- [71] N. Bougdah, S. Bousba, Y. Belhocine, N. Messikh, Application of multilayer perceptron network and random forest models for modelling the adsorption of chlorobenzene on a modified bentonite by intercalation with hexadecyltrimethyl ammonium (HDTMA), *React. Kinet. Mech. Catal.*, 135 (2022) 247–270.
- [72] N. Kaya, Removal of Congo Red and Rhodamine B dyes from aqueous solution using unmodified and NH_3/HCl -modified wood charcoal: a kinetic and thermodynamic study, *Fullerenes Nanotubes Carbon Nanostruct.*, 29 (2021) 183–195.
- [73] H. Zhang, S. Tian, Y. Zhu, W. Zhong, R. Qiu, L. Han, Insight into the adsorption isotherms and kinetics of Pb(II) on pellet biochar via *in-situ* non-destructive 3D visualization using micro-computed tomography, *Bioresour. Technol.*, 358 (2022) 127406, doi: 10.1016/j.biortech.2022.127406.
- [74] N. Bougdah, N. Messikh, S. Bousba, F. Djazi, P. Magri, M. Rogalski, Removal of chlorobenzene by adsorption from aqueous solutions on the HDTMA-bentonites as a function of HDTMA/CEC ratio, *Curr. Res. Green Sustainable Chem.*, 3 (2020) 100038, doi: 10.1016/j.crgsc.2020.100038.
- [75] S. Bousba, N. Bougdah, N. Messikh, P. Magri, Adsorption removal of humic acid from water using a modified Algerian bentonite, *Phys. Chem. Res.*, 6 (2018) 613–625.
- [76] Z. Aksu, Determination of the equilibrium, kinetic and thermodynamic parameters of the batch biosorption of nickel(II) ions onto *Chlorella vulgaris*, *Process Biochem.*, 38 (2002) 89–99.
- [77] M. Adel, M.A. Ahmed, A.A. Mohamed, Effective removal of indigo carmine dye from wastewaters by adsorption onto mesoporous magnesium ferrite nanoparticles, *Environ. Nanotechnol. Monit. Manage.*, 16 (2021) 100550, doi: 10.1016/j.enmm.2021.100550.
- [78] M.A. Ahmed, A.A. Brick, A.A. Mohamed, An efficient adsorption of indigo carmine dye from aqueous solution on mesoporous Mg/Fe layered double hydroxide nanoparticles prepared by controlled sol-gel route, *Chemosphere*, 174 (2017) 280–288.
- [79] J.K. Fatombi, E.A. Idohou, S.A. Osseni, I. Agani, D. Neumeyer, M. Verelst, R. Mauricot, T. Aminou, Adsorption of indigo carmine from aqueous solution by chitosan and chitosan/activated carbon composite: kinetics, isotherms and thermodynamics studies, *Fibers Polym.*, 20 (2019) 1820–1832.
- [80] L. Saikam, P. Arthi, N.D. Jayram, N. Sykam, Rapid removal of organic dyes from aqueous solutions using mesoporous exfoliated graphite, *Diamond Relat. Mater.*, 130 (2022) 109480, doi: 10.1016/j.diamond.2022.109480.